

## Degree of $p$ - $d$ hybridization in $\text{Zn}_{1-x}\text{Mn}_x\text{Y}$ ( $Y=\text{S,Se}$ ) and $\text{Zn}_{1-x}\text{Co}_x\text{S}$ alloys as studied by x-ray-absorption spectroscopy

W. F. Pong

*Department of Physics, Tamkang University, Tamsui, Taiwan 251, Republic of China*

R. A. Mayanovic

*Department of Physics and Astronomy, Southwest Missouri State University, Springfield, Missouri 65804*

J. K. Kao, H. H. Hsieh, J. Y. Pieh, Y. K. Chang, K. C. Kuo, and P. K. Tseng

*Department of Physics, Tamkang University, Tamsui, Taiwan 251, Republic of China*

J. F. Lee

*Synchrotron Radiation Research Center (SRRC), Hsinchu Science-based Industrial Park, Taiwan 300, Republic of China*

(Received 9 August 1996)

We have measured x-ray-absorption near-edge-structure (XANES) spectra of the diluted magnetic semiconductors  $\text{Zn}_{1-x}\text{Mn}_x\text{Y}$  ( $Y=\text{S,Se}$ ) and  $\text{Zn}_{1-x}\text{Co}_x\text{S}$  alloys at the Mn and Co  $L_{3,2}$  edge. Analysis of the Mn  $L_{3,2}$ -edge XANES spectra for  $\text{Zn}_{1-x}\text{Mn}_x\text{Y}$  and Co  $L_{3,2}$ -edge spectra for  $\text{Zn}_{1-x}\text{Co}_x\text{S}$  revealed the presence of a white-line feature in each series, whose intensity increased linearly with concentration  $x$ . The white-line feature is assigned to Mn(Co)  $2p_{3/2}$  and  $2p_{1/2}$  photoelectron excitations to nonbonding  $3d(e)$  states and to the relatively broadened band of Mn (Co)  $3d(t_2)$ -S  $3p$  hybridized antibonding states for the sulfides, and to Mn  $3d(t_2)$ -Se  $4p$  hybridized states for the selenides. The rate of increase of  $L_{3,2}$  white-line intensity with  $x$  is associated with the difference in the degree of  $p$ - $d$  hybridization of states between Mn (Co)  $3d$  and S  $3p$  for the sulfides, and between Mn  $3d$  and Se  $4p$  for the selenides. Our results indicate that the magnetic-transition-metal  $3d(t_2)$ -anion  $p$  hybridization is strongest for  $\text{Zn}_{1-x}\text{Co}_x\text{S}$ , intermediate for  $\text{Zn}_{1-x}\text{Mn}_x\text{S}$  and least for  $\text{Zn}_{1-x}\text{Mn}_x\text{Se}$ . From separate and Co  $K$ -edge extended x-ray-absorption fine-structure measurements on  $\text{Zn}_{1-x}\text{Mn}_x\text{S}$  and  $\text{Zn}_{1-x}\text{Co}_x\text{S}$  at 77 K, we found that the nearest-neighbor (NN) Mn-S (2.42 Å) and Co-S (2.30 Å) bond lengths remained essentially constant with  $x$  in these alloys, respectively. The degree of relaxation of the NN Mn (Co)-anion bond lengths is found to be directly related to the strength of  $p$ - $d$  hybridization coupling in these alloys. [S0163-1829(97)00411-6]

### I. INTRODUCTION

One of the more interesting classes of materials to exhibit a wide range of unique electrical, magnetic, and optical properties are diluted magnetic semiconductors (DMS's). As their name suggests, DMS's result from the alloying of magnetic transition metals and semiconducting compounds. The most widely studied II-VI-based DMS's have been those containing  $\text{Mn}^{2+}$  as the substitutional magnetic cation.<sup>1</sup> In recent years, Fe- and Co-based DMS's have also been successfully grown and extensively investigated.<sup>2</sup> It is widely accepted that some of the more important types of investigations made on II-VI-based DMS's have concentrated on systematic studies of their electronic band structure, and how it is affected by the type of anion and both by the type and relative concentration of host group-II cation and substitutional magnetic ion. Photoemission spectroscopy studies of  $\text{Mn}^{2+}$   $3d$  states in  $\text{Cd}_{1-x}\text{Mn}_x\text{Y}$  ( $Y=\text{S, Se, Te}$ ),<sup>3</sup> showed that the  $\text{Mn}^{2+}$   $3d$  partial density of states extends over all the valence bands as a result of strong  $p$ - $d$  hybridization, which was inferred to vary in two important ways: (1) The amount of  $p$ - $d$  hybridization increases directly with Mn concentration  $x$ , and (2) it increases in going from  $\text{Te}\rightarrow\text{Se}\rightarrow\text{S}$  in the series. This is attributed to the difference between the Mn  $3d(t_2)$  and anion  $p$ -state energy levels, varying systemati-

cally both with Mn concentration and anion type. It should be noted that controversy still exists concerning the different degree of hybridization between Mn  $3d$  and anion  $p$  orbitals in the  $\text{Zn}_{1-x}\text{Mn}_x\text{Y}$  ( $Y=\text{S,Se,Te}$ ) series.<sup>4</sup> Theoretical calculations showed that the hybridization energy between the  $\text{Mn}^{2+}$   $3d$  and local anion  $p$ -level valence electrons increases slightly in going from  $\text{Te}\rightarrow\text{Se}\rightarrow\text{S}$  for both  $\text{Cd}_{1-x}\text{Mn}_x\text{Y}$  and  $\text{Zn}_{1-x}\text{Mn}_x\text{Y}$  ( $Y=\text{S,Se,Te}$ ) systems.<sup>5</sup> This was also supported by the electronic band-structure calculations.<sup>6</sup> Obviously, the electronic band structure of a solid is directly affected by its physical structure, and vice versa. Accordingly, DMS lattice constants were found to decrease in going from  $\text{Te}\rightarrow\text{Se}\rightarrow\text{S}$  in  $\text{Cd}_{1-x}\text{Mn}_x\text{Y}$ , in agreement with a model for which the amount of  $p$ - $d$  orbital overlap is directly determined by the size of the anion.<sup>3,7</sup>

Our results from extended x-ray-absorption fine-structure (EXAFS) studies<sup>8,9</sup> were found to be consistent with tetrahedral bond weakening in these and other Mn-based DMS alloys. The bond weakening was attributed to Mn  $3d$ - and anion  $p$ -orbital hybridization, which in turn causes a decreased amount of charge to be available for the making of  $sp^3$  bonds. More recently, we discovered a concentration and magnetic-transition-metal-type-dependent preedge resonance peak in the S  $K$ -edge x-ray-absorption near-edge structure (XANES) spectra of  $\text{Zn}_{1-x}\text{M}_x\text{S}$  ( $M=\text{Mn,Fe,Co}$ ),<sup>10</sup> which

was attributed to S  $1s$  photoelectron excitations to the unoccupied S  $3p$ –M  $3d(t_2)$  hybridized antibonding states. Given this interpretation, the main density of M  $3d$ –S  $3p$  hybridized states above the Fermi level should be observable for all excitations involving final anion outermost  $p$  states or final  $M^{2+}$   $3d$  states in  $Zn_{1-x}M_xY$  systems, including those for which the magnetic-transition-metal ion is excited in the photoionization and excitation process. Our primary goal in this study was to verify our previous findings from S  $K$ -edge XANES spectra for  $Zn_{1-x}M_xS$ , but in this case having chosen the magnetic-transition-metal ion for photoexcitation. In addition, we chose to study the effect of anion size influencing the  $p$ - $d$  hybridization between Mn and S and Co and S for the sulfides, and between Mn and Se for the selenides. Since the tetrahedral radius of the  $S^{2-}$  ion in DMS's is considerably smaller than that of the  $Se^{2-}$  ion, the DMS systems  $Zn_{1-x}Mn_xS$  and  $Zn_{1-x}Mn_xSe$  can provide a suitable combination of systems in which to study the effect of the anion on their microstructure and, thereby, on details of their electronic band structure. We first discuss our results based on Mn  $L_{3,2}$ -edge XANES measurements made on  $Zn_{1-x}Mn_xY$  ( $Y=S,Se$ ) and Co  $L_{3,2}$ -edge XANES measurements made on  $Zn_{1-x}Co_xS$  alloys. Our quantitative analysis of the  $L_3$  and  $L_2$  white-line intensity of these spectra was used in order to interpret the results of different degree of Mn (Co)  $3d$ -anion  $p$  hybridization in our DMS systems. An auxiliary study of the nearest-neighbor (NN) Mn-S bond lengths in  $Zn_{1-x}Mn_xS$  and Co-S bond lengths in  $Zn_{1-x}Co_xS$ , from Mn and Co  $K$ -edge EXAFS measurements made on these alloys,<sup>11</sup> respectively, is also discussed. The results support the hypothesis that the degree of relaxation of the NN Mn (Co)-anion bond lengths is strongly associated with the strength of  $p$ - $d$  hybridization coupling.

## II. EXPERIMENT

XANES spectra of  $Zn_{1-x}Mn_xY$  ( $Y=S,Se$ ) have been measured at the Mn  $L_{3,2}$  edge and  $Zn_{1-x}Co_xS$  at the Co  $L_{3,2}$  edge at the Synchrotron Radiation Research Center (SRRC), Hsinchu, Taiwan, using a high-energy spherical grating monochromator (HSGM) beamline with an electron-beam energy of 1.3 GeV and a maximum stored current of 200 mA. The grating (1200 l/mm) is made of gold-coated fused silica, and covers a photon-energy range from 400 to 1200 eV. The spectra were measured using the sample current mode at room temperature, under a base pressure of better than  $5 \times 10^{-9}$  torr. Photon energies for all Mn and Co  $L_{3,2}$ -edge XANES spectra, having an energy resolution of  $\sim 0.4$  eV, were calibrated using the well-known spectrum of the  $CaF_2$  thin film. The  $Zn_{1-x}Mn_xY$  ( $Y=S,Se$ ) samples were grown using Bridgman's technique while the  $Zn_{1-x}Co_xS$  were grown using the chemical vapor transport method. The single phase and concentration of the samples were confirmed using x-ray diffraction and energy-dispersive x-ray fluorescence analysis. The concentration for the  $Zn_{1-x}Mn_xS$  alloy samples were  $x=0.06, 0.13, 0.23,$  and  $0.40$ ; for  $Zn_{1-x}Mn_xSe$ ,  $x=0.08, 0.25,$  and  $0.44$ ; and for  $Zn_{1-x}Co_xS$ ,  $x=0.03, 0.10, 0.20,$  and  $0.30$ . The samples were ground and sieved to find powders having particle size  $< 400$  mesh (each particle  $< 38 \mu m$  in diameter) and put onto an

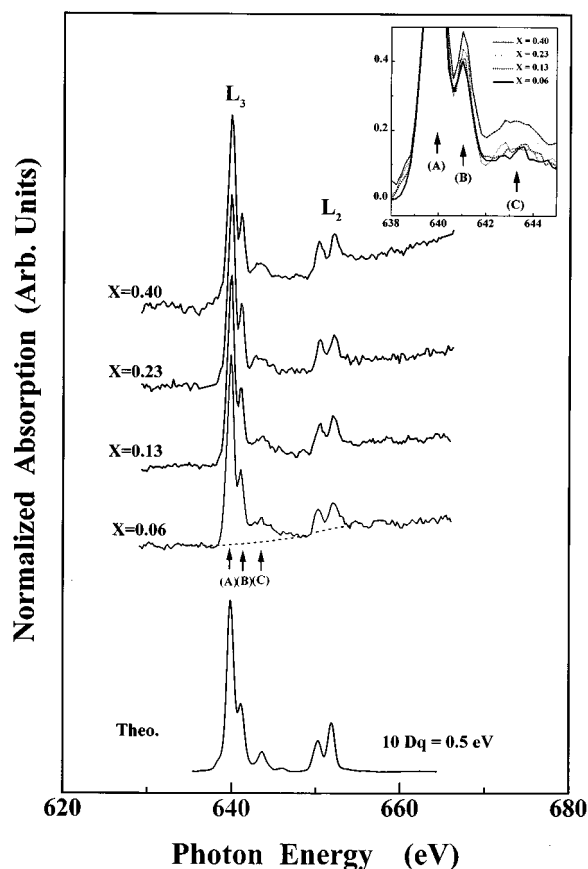


FIG. 1. Normalized Mn  $L_{3,2}$ -edge absorption spectra of  $Zn_{1-x}Mn_xS$ . The white-line region of the Mn  $L_3$  edge is inset on a magnified scale. The multiplet spectrum was calculated assuming a  $3d^5$  ground state with  $10Dq=0.5$  eV (from Ref. 13).

adhesive indium tape for sample current measurements. All measurements were made at room temperature.

## III. RESULTS AND DISCUSSIONS

Figures 1 and 2 show the Mn  $L_{3,2}$ -edge XANES spectra of  $Zn_{1-x}Mn_xY$  ( $Y=S,Se$ ) and Fig. 3 shows the Co  $L_{3,2}$ -edge XANES spectra of  $Zn_{1-x}Co_xS$ . All of the spectra shown have been normalized by the incident intensity  $I_0$  and, after subtraction of preedge background at the  $L_3$  edge, scaled by the maximum of the peak heights (labeled A) to unity at the absorption edge. Using the dipole-selection transition rule, we attribute the white line features at the Mn (Co)  $L_{3,2}$ -edge (labeled  $L_3$  and  $L_2$ ) XANES to photoelectron transitions from the  $Mn^{2+}$  ( $Co^{2+}$ )  $2p_{3/2}$  and  $2p_{1/2}$  ground states to the final unoccupied  $Mn^{2+}$  ( $Co^{2+}$ )  $3d$  electron states. The shape of the  $Zn_{1-x}Mn_xY$  ( $Zn_{1-x}Co_xS$ ) alloys' spectra were found to be nearly identical at Mn (Co)  $L_{3,2}$  edge throughout the range of  $x$  values in each series. In contrast to the generally single-peaked feature observed at the Co  $L_{3,2}$ -edge XANES spectra of  $Zn_{1-x}Co_xS$ , a rather complicated Mn  $L_{3,2}$ -edge XANES spectra of  $Zn_{1-x}Mn_xY$  was observed, exhibiting strong multiplet and crystal effects.<sup>12,13</sup> As seen in Figs. 1 and 2, peak A is accompanied by a lower-intensity peak (labeled B) located just above the Mn  $L_3$  edge, while the  $L_2$ -edge white-line feature exhibits a peak doublet,

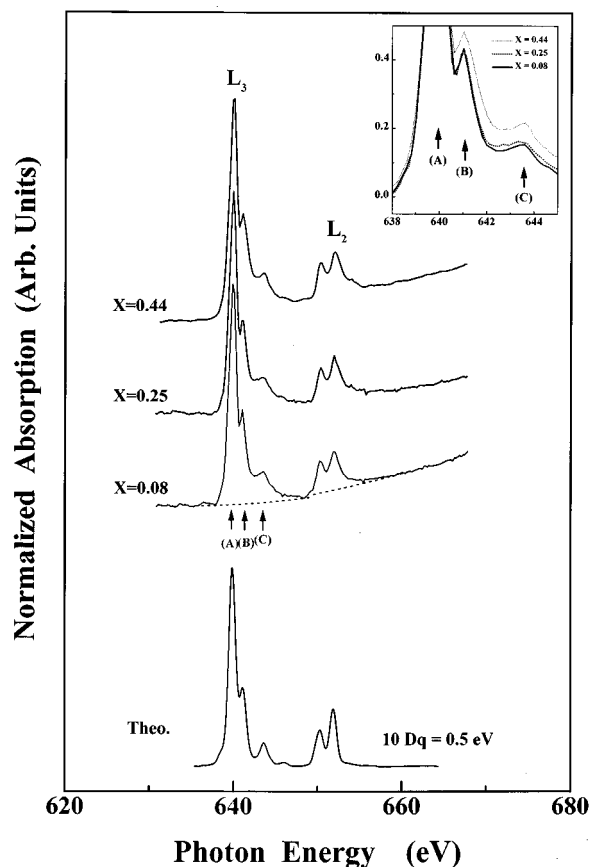


FIG. 2. Normalized Mn  $L_{3,2}$ -edge absorption spectra of  $Zn_{1-x}Mn_xSe$ . The white-line region of the Mn  $L_3$  edge is inset on a magnified scale. The multiplet spectrum was calculated assuming a  $3d^5$  ground state with  $10Dq=0.5$  eV (from Ref. 13).

in both  $Zn_{1-x}Mn_xS$  and  $Zn_{1-x}Mn_xSe$  alloys. Conversely, the Co  $L_{3,2}$ -edge white-line features of  $Zn_{1-x}Co_xS$  (Fig. 3) are exhibited as relatively broad, individual peaks, respectively. The full width at half maximum (FWHM) of peak A was found to be  $\sim 1.1$  eV for  $Zn_{1-x}Mn_xY$ , irrespective of  $x$ , while for peak B it was found to increase uniformly from  $\sim 0.36$  eV at  $x=0.06$  to  $\sim 0.50$  eV at  $x=0.40$ , and from  $\sim 0.29$  eV at  $0.08$  to  $\sim 0.40$  eV at  $x=0.44$  for  $Zn_{1-x}Mn_xS$  and  $Zn_{1-x}Mn_xSe$  alloys, respectively (see the insets of Figs. 1 and 2). The FWHM of peak A increased uniformly from 2.0 eV at  $x=0.06$  to 2.3 eV at  $x=0.30$  for  $Zn_{1-x}Co_xS$  (see the inset of Fig. 3). The relatively broader FWHM of peak A for  $Zn_{1-x}Co_xS$  can be attributed to peaks A and B, in the case of Mn  $L_{3,2}$ -edge XANES spectra of  $Zn_{1-x}Mn_xY$ , being unresolved at the Co  $L_3$  edge. Similar results for the variation of the white-line intensity with Fe concentration were also reported from Fe  $L_3$ -edge absorption measurement made on  $Zn_{1-x}Fe_xS$  alloys.<sup>14</sup> In addition, the high-energy satellite structure (labeled C), occurring  $\sim 3$  eV above the Mn and Co  $L_3$ -edge main features in the XANES spectra, have been observed as occurring more pronouncedly for  $Zn_{1-x}Mn_xY$ , and less pronouncedly in  $Zn_{1-x}Co_xS$ . The intensity of this satellite structure was found to basically increase with  $x$ , and is presumably caused by the excitation of Mn (Co)  $2p_{3/2}$  photoelectrons to  $4s$  states in the conduction band.<sup>15</sup> Van der Laan and Kirkman calculated theoretical  $L_{3,2}$ -edge absorption spectra of first-row transition-metal ions

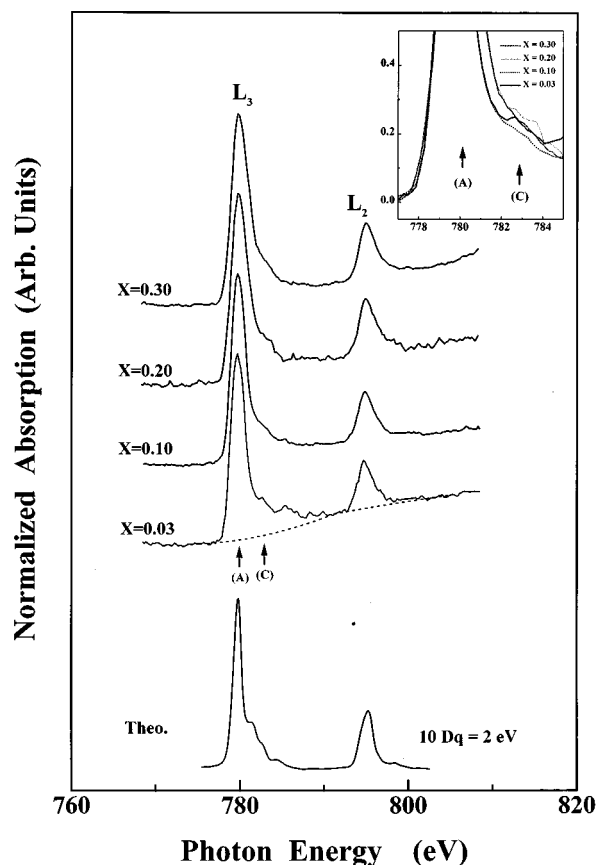


FIG. 3. Normalized Co  $L_{3,2}$ -edge absorption spectra of  $Zn_{1-x}Co_xS$ . The white-line region of the Co  $L_3$  edge is inset on a magnified scale. The multiplet spectrum was calculated assuming a  $3d^7$  ground state with  $10Dq=2.0$  eV (from Ref. 13).

in tetrahedral and octahedral crystal-field symmetry, respectively, based on the atomic multiplet theory.<sup>13</sup> They approximated the effects due to the cubic crystal field by use of ligand-field splitting parameter  $10Dq$  ranging from 0 to 3 eV in increments of 0.5 eV. We have selected on the basis of best agreement with our experimental spectra, and included in Figs. 1–3, the theoretical XANES spectra of Van der Laan and Kirkman having  $10Dq=0.5$  and 2 eV (in the tetrahedral symmetry  $T_d$ ) (Ref. 13) for Mn and Co  $L_{3,2}$  edges, respectively, for  $Zn_{1-x}Mn_xY$  and  $Zn_{1-x}Co_xS$  alloys. The maximum intensity peak of the theoretical  $L_3$ -edge spectra has been aligned in each case with peak A of the experimental spectra. Note that the line shape of the theoretical spectra is strongly dependent on  $10Dq$ , meaning that the strength of ligand field strongly affects the final-state multiplet.<sup>12,13</sup>

Our results can be explained with greater clarity using Fig. 4, which was adopted from Fig. 6 of Ref. 10 and which shows a schematic representation of the Mn  $3d$  (Co  $3d$ ), S  $3p$ , and Se  $4p$  bands of  $Zn_{1-x}Mn_xS$  ( $Zn_{1-x}Co_xS$ ) and  $Zn_{1-x}Mn_xSe$  alloys derived from their respective atomic levels. Because the structure surrounding  $Mn^{2+}$  ( $Co^{2+}$ ) ions in  $Zn_{1-x}Mn_xY$  ( $Zn_{1-x}Co_xS$ ) exhibits  $T_d$  group symmetry, the magnetic-transition-metal  $3d$  states are split into  $e$  doublets (having lower energy than the undistorted  $3d$  orbitals) and  $t_2$  triples (having higher energy than the undistorted  $3d$  orbitals) by the crystal field. Due to  $3p$  ( $4p$ ) electrons on neighboring S (Se) atoms having  $t_2$  symmetry, there is no

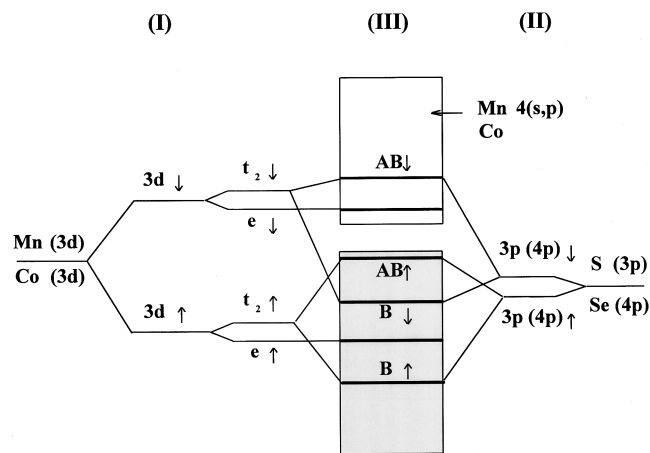


FIG. 4. Schematic energy diagram showing respective atomic levels forming Mn (Co)  $3d$  and S  $3p$  (Se  $4p$ ) bands. (I) Exchange and ligand-field splitting of Mn (Co)  $3d$  states. (II) Exchange splitting of S  $3p$  (Se  $4p$ ) states. (III) The final hybridized states. AB and B denote antibonding and bonding states, respectively.  $\uparrow$  and  $\downarrow$  denote states for spin-up and spin-down, respectively (not to scale).

$p$ - $d$  hybridization for the Mn (Co)  $3d(e)$  states on symmetry grounds. Therefore, the  $3d(e)$  levels remain local, as is shown by the fact that the peak in the XANES spectra associated with photoexcitations of  $2p$  electrons to these final states remains dispersionless with  $x$ . In contrast, the  $3d(t_2)$  are strongly hybridized with the S  $3p$  (Se  $4p$ ) states of the same symmetry, and contribute to the broadening of bands derived from these states in the spectra. As mentioned above we attribute the white-line feature of Mn (Co)  $L_{3,2}$  edge to dipole-allowed transitions of photoelectrons from  $\text{Mn}^{2+}$  ( $\text{Co}^{2+}$ )  $2p_{3/2}$  and  $2p_{1/2}$  states to the unoccupied  $3d$  states above the Fermi level. More specifically a reasonable conclusion is that the white-line feature of the  $L_{3,2}$  edge corresponds predominantly to Mn (Co)  $2p_{3/2}$  and  $2p_{1/2}$  electrons making transitions to a relatively narrow band of Mn (Co)  $3d(e)$  and to a broadened band of Mn (Co)  $3d(t_2)$ -S  $3p$  hybridized antibonding states for the sulfides, and to Mn  $3d(t_2)$ -Se  $4p$  hybridized states for the selenides.

The strength of  $p$ - $d$  hybridization in DMS alloys, being predominantly determined by the degree of overlap of the appropriate  $p$ - and  $d$ -orbital wave functions, should be reflected in the electronic transition probabilities occurring between the same  $p$ - and  $d$ -derived states.<sup>10</sup> In order to test this, we calculated the integrated intensity of the white-line features at the  $L_2$  and  $L_3$  edges (excluding feature C) of our spectra. Specifically, we have tried to determine from these results how the strength of  $p$ - $d$  hybridization varies as a function of content and type of magnetic ion and anion making up the DMS alloys. The first step in the analysis involved the removal of a linear background from the  $L_2$ - and  $L_3$ -edge regions (indicated by the dashed lines in Figs. 1–3); The Mn and Co  $L_2$ -edge XANES spectra with subtracted background are presented in Fig. 5. Note that prior to analysis of the integrated intensities, the spectra were normalized, as described above, to  $I_0$  and to the maximum of peak A of the  $L_3$ -edge region. As can be seen in Fig. 5, the intensity of the  $L_2$  white-line feature increases with magnetic-transition-metal content Mn (Co) in  $\text{Zn}_{1-x}\text{Mn}_x\text{Y}$  ( $\text{Zn}_{1-x}\text{Co}_x\text{S}$ ) alloys. In order to attain reasonable comparison of their intensities

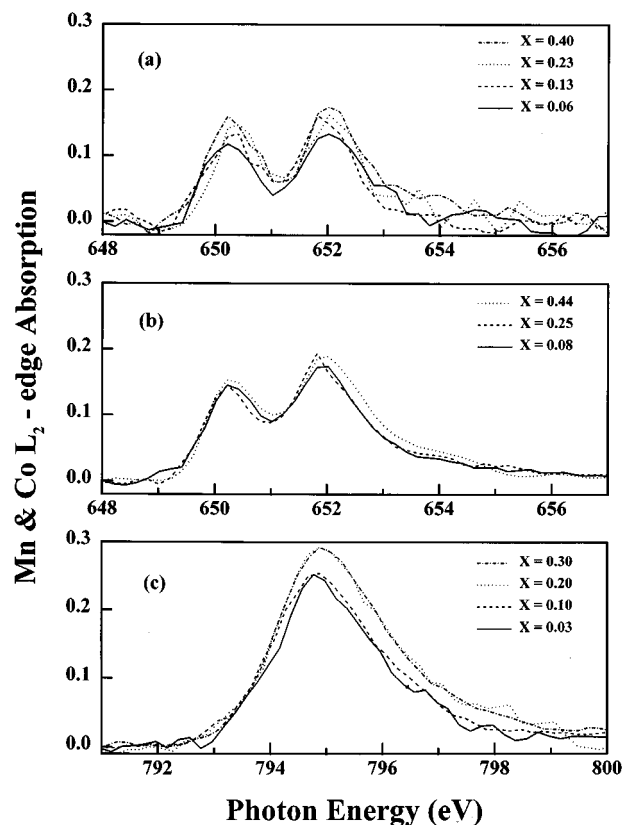


FIG. 5. The white-line spectra of (a) the Mn  $L_2$  edge for  $\text{Zn}_{1-x}\text{Mn}_x\text{S}$  and (b)  $\text{Zn}_{1-x}\text{Mn}_x\text{Se}$ , and (c) for the Co  $L_2$  edge for  $\text{Zn}_{1-x}\text{Co}_x\text{S}$ .

within the same energy scale, the  $L_2$  white-line intensities were integrated between 649.5 and 653.5 eV for  $\text{Zn}_{1-x}\text{Mn}_x\text{Y}$  and between 793.5 and 797.5 eV for  $\text{Zn}_{1-x}\text{Co}_x\text{S}$ . Our results for the variation of the integrated intensity of the  $L_2$  white-line feature as a function of  $x$  are plotted in Fig. 6: The linear-regression slope and intercept values of fitted lines are given in Table I. The analysis of the  $L_3$  edge was complicated somewhat by the overlap of peaks A, B, and C, the last being attributed to excitations involving final-state Mn (Co)  $4s$  bands. The intensities of overlapping features occurring at the  $L_3$  edge were integrated between 638.3 and 641.7 eV for  $\text{Zn}_{1-x}\text{Mn}_x\text{Y}$  and between 777.6 and 781.8 eV for  $\text{Zn}_{1-x}\text{Co}_x\text{S}$  using multiple-peak analysis: Examples of the peak fitting used for the analysis of the  $L_3$ -edge features are shown in Fig. 7. Since feature C is associated with excitations of photoelectrons to  $4s$  states, its integrated intensity was used only to isolate the contributions of features A and B for  $\text{Zn}_{1-x}\text{Mn}_x\text{Y}$  and the contribution of feature A for  $\text{Zn}_{1-x}\text{Co}_x\text{S}$ . In similar fashion to the integrated intensity of the  $L_2$  white-line feature, the combined intensities of features A and B ( $I_A + I_B$ ) occurring at the Mn (Co)  $L_3$  edge and the intensity of feature A ( $I_A$ ) occurring at the Co  $L_3$  edge were found to increase linearly with magnetic-transition-metal concentration in  $\text{Zn}_{1-x}\text{Mn}_x\text{Y}$  and in  $\text{Zn}_{1-x}\text{Co}_x\text{S}$  alloys, respectively. The variation of the  $L_3$  white-line intensities  $I_A + I_B$  for  $\text{Zn}_{1-x}\text{Mn}_x\text{Y}$  and  $I_A$  for  $\text{Zn}_{1-x}\text{Co}_x\text{S}$  as a function of  $x$  are plotted in Fig. 8: The slope and intercept values from fitting the data represented in this graph using linear regression are given in Table II. We note

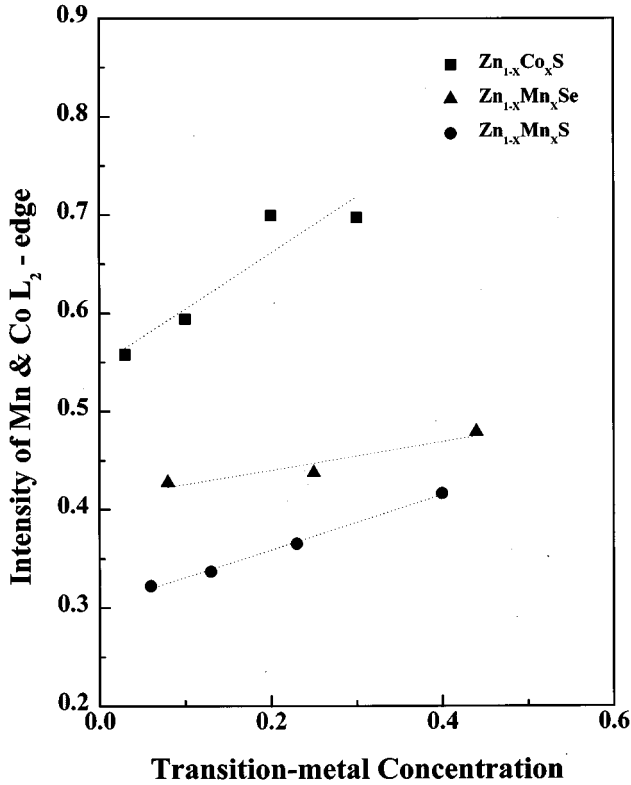


FIG. 6. The intensity of white-line spectra at the  $L_2$  edge and fit using linear regression as a function of magnetic-transition-metal concentration for  $\text{Zn}_{1-x}\text{Mn}_x\text{S}$ ,  $\text{Zn}_{1-x}\text{Mn}_x\text{Se}$ , and  $\text{Zn}_{1-x}\text{Co}_x\text{S}$  alloys.

that the energy range of integration of the  $L_3$ -edge features is 0.8 eV larger for  $\text{Zn}_{1-x}\text{Co}_x\text{S}$  in comparison to that for  $\text{Zn}_{1-x}\text{Mn}_x\text{Y}$ , leading to greater overall  $L_3$  white-line intensities for the former than for the latter (aside from the  $x$  dependence for both). Nevertheless, this difference in energy range was found to have no impact on the  $x$  dependence of the  $L_3$  white-line intensity for  $\text{Zn}_{1-x}\text{Co}_x\text{S}$  in comparison to that for  $\text{Zn}_{1-x}\text{Mn}_x\text{Y}$ .

The linear increase of the integrated intensities of features at the Mn (Co)  $L_3$  and  $L_2$  edges with Mn (Co) concentration can be explained by the overall number of Mn (Co)  $2p_{3/2}$  and  $2p_{1/2}$  to Mn (Co)  $3d(t_2)$ -anion  $p$  hybridized states' transitions similarly increasing linearly with  $x$ , respectively, because proportionally more Mn (Co)  $3d(t_3)$  orbitals become available for hybridization with anion  $p$  orbitals. In addition, we find that within the concentration ranges we studied, the rate of increase in intensity of white-line features occurring at the  $L_{3,2}$  edge with  $x$  is dependent upon both the type of substitutional magnetic ion and type of anion in our DMS

TABLE I. Slope and intercept of the line fitted using linear regression to the intensity of the white line as a function of concentration from (a) the Mn  $L_2$  edge for  $\text{Zn}_{1-x}\text{Mn}_x\text{S}$  and (b)  $\text{Zn}_{1-x}\text{Mn}_x\text{Se}$ , and (c) for the Co  $L_2$  edge for  $\text{Zn}_{1-x}\text{Co}_x\text{S}$  alloys.

|           | $\text{Zn}_{1-x}\text{Mn}_x\text{S}$ | $\text{Zn}_{1-x}\text{Mn}_x\text{Se}$ | $\text{Zn}_{1-x}\text{Co}_x\text{S}$ |
|-----------|--------------------------------------|---------------------------------------|--------------------------------------|
| Slope     | $0.28 \pm 0.01$                      | $0.15 \pm 0.05$                       | $0.57 \pm 0.16$                      |
| Intercept | $0.30 \pm 0.01$                      | $0.41 \pm 0.01$                       | $0.55 \pm 0.03$                      |

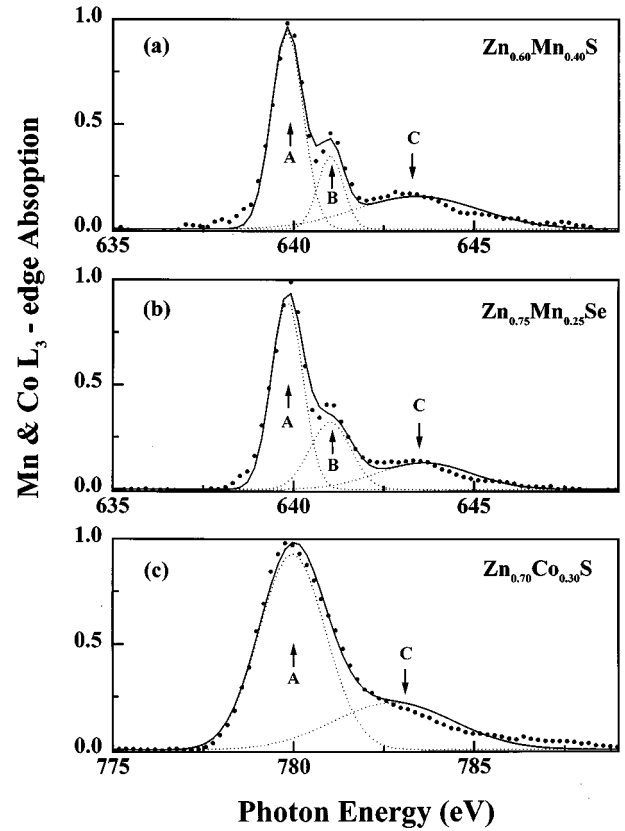


FIG. 7. Experimental (solid circles) and fitted data of white-line spectra at (a) the Mn  $L_3$  edge for  $\text{Zn}_{0.6}\text{Mn}_{0.4}\text{S}$  and (b)  $\text{Zn}_{0.75}\text{Mn}_{0.25}\text{Se}$ , and (c) for the Co  $L_3$  edge for  $\text{Zn}_{0.7}\text{Co}_{0.3}\text{S}$ . The final fitting curves (solid lines) were calculated by a summation of three-peak curves, namely, for A, B, and C (two-peak A and C) for  $\text{Zn}_{0.6}\text{Mn}_{0.4}\text{S}$  and  $\text{Zn}_{0.75}\text{Mn}_{0.25}\text{Se}$  ( $\text{Zn}_{0.7}\text{Co}_{0.3}\text{S}$ ), with the individual peak curves shown by the dashed lines.

systems. We first make a comparison of our results for the two types of magnetic ions in the  $\text{Zn}_{1-x}\text{Co}_x\text{S}$  and  $\text{Zn}_{1-x}\text{Mn}_x\text{S}$  alloys. The rate of increase in  $L_3$ - and  $L_2$ -edge white-line intensity with  $x$  for  $\text{Zn}_{1-x}\text{Co}_x\text{S}$  is roughly 2–3 times as much as for  $\text{Zn}_{1-x}\text{Mn}_x\text{S}$ , as shown in Tables I and II, indicating that transition-metal  $3d(t_2)$ -S  $3p$  hybridization is stronger for  $\text{Zn}_{1-x}\text{Co}_x\text{S}$  than for  $\text{Zn}_{1-x}\text{Mn}_x\text{S}$ . This suggests that the Co  $3d(t_2)$  energy levels, in comparison with the Mn  $3d(t_2)$  energy levels, are situated nearer to S  $3p$  states, and thus have a higher hybridization probability with the S  $3p$  states. This conclusion is consistent with our earlier S  $K$ -edge XANES study of  $\text{Zn}_{1-x}\text{M}_x\text{S}$  alloys ( $M = \text{Mn, Fe, Co}$ ), in which we obtained similar results for a preedge resonance peak.<sup>10</sup> Inferences on the effect of the type of anion on the strength of  $p$ - $d$  hybridization in our DMS alloys are not as apparent. Based on the rate of increase of the Mn  $L_2$ -edge white-line intensity with  $x$  being roughly twice for  $\text{Zn}_{1-x}\text{Mn}_x\text{S}$  compared to that of  $\text{Zn}_{1-x}\text{Mn}_x\text{Se}$ , we infer that S has a greater effect than Se. More specifically, this result suggests that Mn  $3d(t_2)$ -S  $3p$  hybridization for  $\text{Zn}_{1-x}\text{Mn}_x\text{S}$  is stronger than Mn  $3d(t_2)$ -Se  $4p$  for  $\text{Zn}_{1-x}\text{Mn}_x\text{Se}$ . However, given that the rate of increase of the Mn  $L_3$ -edge white-line intensity with  $x$ , being equal for  $\text{Zn}_{1-x}\text{Mn}_x\text{S}$  compared to that of  $\text{Zn}_{1-x}\text{Mn}_x\text{Se}$  (see Table II), one would have to infer that S and Se have roughly the same effect. It is highly possible, given that the error in estimation

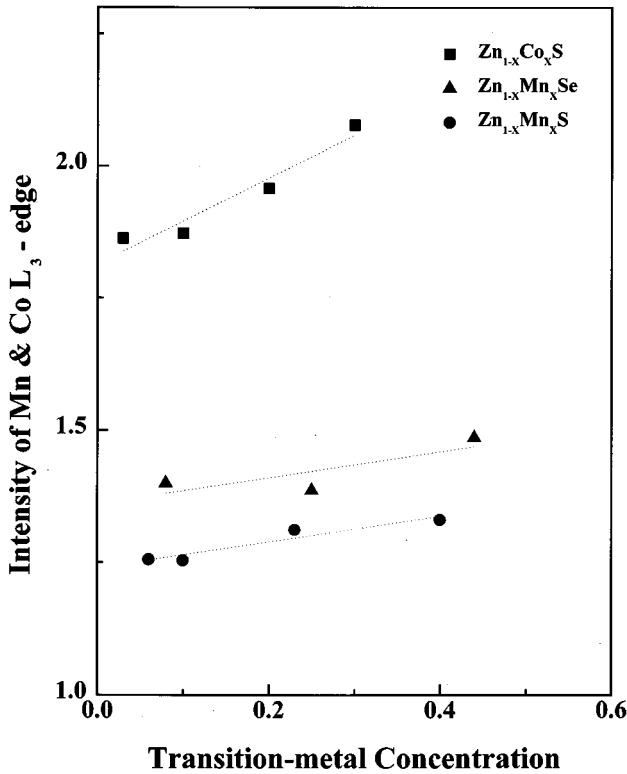


FIG. 8. The intensity of white-line spectral  $I_A + I_B$  ( $I_A$ ) at the  $L_3$  edge and the linear regression fitting as a function of magnetic-transition-metal concentration for  $Zn_{1-x}Mn_xS$  and  $Zn_{1-x}Mn_xSe$  ( $Zn_{1-x}Co_xS$ ) alloys.

of integrated intensity of the Mn  $L_3$ -edge white-line intensity with  $x$  is lower and thus more in line with the results for the  $L_3$  edge. This conjecture is supported by the excellent agreement of the rates of increase of the Mn and Co  $L_{3,2}$  edge white-line intensities with  $x$  for  $Zn_{1-x}Mn_xS$  and  $Zn_{1-x}Co_xS$  alloys, respectively. Combining these results, we conclude that the magnetic-transition-metal  $3d(t_2)$ -anion  $p$  hybridization is highest for  $Zn_{1-x}Co_xS$ , intermediate for  $Zn_{1-x}Mn_xS$ , and least for  $Zn_{1-x}Mn_xSe$  alloys. This is consistent with studies showing that the exchange interaction of the magnetic moment in Co-based DMS alloys is several times larger compared to that of Mn-based DMS alloys,<sup>16</sup> and in agreement with similar studies, indicating that the value of the exchange integral decreases with increasing anion size in Mn-based DMS systems.<sup>17</sup>

Possible concerns regarding the quantitative analysis of magnetic-transition-metal  $L_{3,2}$ -edge white-line feature of XANES spectra, which require addressing, (1) the intrinsic

TABLE II. Slope and intercept of the line fitted using linear regression to the intensity of the multiple-peak analysis as a function of concentration from white-line spectra at (a) the Mn  $L_3$  edge for  $Zn_{1-x}Mn_xS$  and (b)  $Zn_{1-x}Mn_xSe$ , and (c) for the Co  $L_3$  edge for  $Zn_{1-x}Co_xS$ .

|           | $Zn_{1-x}Mn_xS$ | $Zn_{1-x}Mn_xSe$ | $Zn_{1-x}Co_xS$ |
|-----------|-----------------|------------------|-----------------|
| Slope     | $0.25 \pm 0.05$ | $0.25 \pm 0.17$  | $0.82 \pm 0.15$ |
| Intercept | $1.25 \pm 0.01$ | $1.36 \pm 0.05$  | $1.81 \pm 0.03$ |

and instrumental broadening, and (2) final-state effects such as core excitations or shake-off processes.<sup>18</sup> The core-hole broadening of the white-line feature for Mn and Co  $L_2$ -edge ( $L_3$ -edge) spectra is 0.34 and 0.43 eV (0.2 and 0.3 eV), respectively,<sup>19</sup> whereas, as discussed in the previous section, the instrumental broadening for our x-ray-absorption measurements was  $\sim 0.4$  eV. The contribution to the broadening due to shake-off and excitonic effects is expected to be similar to that of core-hole broadening.<sup>18</sup> While core-hole broadening has been shown to be dependent upon the state of aggregation of the absorbing element in some systems,<sup>20</sup> we do not expect this and other final state and intrinsic effects to contribute to the broadening of the spectra in question, specifically regarding effects which are  $x$  dependent. Therefore, we conclude that core-hole lifetime and final-state effects, while present are not dominantly responsible for the observed rate of increase in Mn (Co)  $L_{3,2}$ -edge white-line intensity with  $x$  in the spectra. One possible explanation for the intensity of the Co  $L_{3,2}$ -edge white line for  $Zn_{1-x}Co_xS$  being nominally larger than that of Mn  $L_{3,2}$ -edge for  $Zn_{1-x}Mn_xY$  (aside from their respective  $x$  dependence) is because the core-hole broadening for the former is slightly larger than that of the latter.<sup>21</sup> On the other hand, we cannot offer any similar explanation for the overall intensity of Mn  $L_{3,2}$ -edge white line in the XANES spectra of  $Zn_{1-x}Mn_xSe$  being slightly larger than that for  $Zn_{1-x}Mn_xS$ .

In a separate study, the Mn and Co  $K$ -edge EXAFS spectra were measured from  $Zn_{1-x}Mn_xS$  and  $Zn_{1-x}Co_xS$  alloys using transmission mode measurements at 77 K.<sup>11</sup> We found that the NN  $M$ -S bond lengths remained essentially constant at 2.42 Å in  $Zn_{1-x}Mn_xS$  (Mn-S) and at 2.30 Å in  $Zn_{1-x}Co_xS$  (Co-S) throughout the concentration range of  $x$ , respectively. Results for NN bond lengths, nearly completely independent of  $x$  in  $Zn_{1-x}Mn_xS$  (Ref. 22) and  $Zn_{1-x}Co_xS$ <sup>23</sup> have been observed earlier. Similar results have also been found for the NN Mn-Se bond lengths (having a value of 2.54 Å) in  $Zn_{1-x}Mn_xSe$  from our earlier EXAFS studies.<sup>8</sup> In contrast to the NN Mn-anion bond lengths in  $Zn_{1-x}Mn_xS$  and  $Zn_{1-x}Mn_xSe$  which remain nearly  $x$  independent, the mean cation-cation distances in these and other DMS alloys have been found to obey Vegard's law,<sup>24</sup> implying a distortion of the crystal structure away from the ideal structure conforming to Vegard's law.<sup>8,9</sup> From this, we inferred that the  $Mn^{2+}$  ion played a significant role in weakening tetrahedral  $sp^3$  bonds in Mn-based DMS's.<sup>8,9</sup> Since the NN Co-S bond length is also found to be nearly  $x$  independent, we can safely generalize the previous conclusion to include the effect that the  $Co^{2+}$  ion has on similar  $sp^3$  bonds in  $Zn_{1-x}Co_xS$  alloys. The  $sp^3$  bond weakening is due to the strong hybridization of  $Mn^{2+}$  ( $Co^{2+}$ )  $3d$  orbitals having  $t_2$  symmetry with anion  $3p$  or  $4p$  orbitals. The atomic energy degeneracy necessary for the superexchange mechanism in DMS leaves fewer anion  $p$  orbitals available for tetrahedral bonding, thus causing a reduction in the bond force constants.<sup>7,25</sup> Similar conclusions by Qadri *et al.*<sup>26</sup> showed that  $Mn^{2+}$  tends to weaken the tetrahedral bond and to destabilize the zinc-blende structure. Although the NN Mn-anion bond lengths are nearly  $x$  independent, it should be pointed out that a careful EXAFS analysis of these bond lengths for both  $Zn_{1-x}Mn_xS$  and  $Zn_{1-x}Mn_xSe$  has shown a slightly greater  $x$  dependence in the latter than in the

former (from their NN bond-length relaxation data; see Table II of Ref. 9). This reveals a greater deviation in  $Zn_{1-x}Mn_xS$  than in  $Zn_{1-x}Mn_xSe$  of the local structure away from Vegard's law behavior. This difference may arise because of the greater size of the Se (the covalent radius is equal to 1.16 Å) than the S (the covalent radius is equal to 1.02 Å) anion, resulting in greater  $p$ - $d$  hybridization (and concomitant greater weakening of the tetrahedral  $sp^3$  bond) in  $Zn_{1-x}Mn_xS$  than in  $Zn_{1-x}Mn_xSe$  alloys. Finally, according to Spalek *et al.*,<sup>27</sup> the superexchange integral in Mn-based DMS's should depend on the amount of Mn-anion-Mn bond-angle distortion. Since we have evidence of a linear  $x$  dependence of the Mn-Se-Mn bond-angle distortion in  $Zn_{1-x}Mn_xSe$ ,<sup>8</sup> it should be interesting to determine the nature of the corresponding bond-angle distortion in  $Zn_{1-x}Mn_xS$  and  $Zn_{1-x}Co_xS$ . A more inclusive study of this nature should prove to be useful in determining general effects of the magnetic ion and anion on the bond-angle distortion and its influence on the superexchange mechanism in DMS. Further analysis of the EXAFS data, for the next-nearest-neighbor distances in the  $Zn_{1-x}Mn_xS$  and  $Zn_{1-x}Co_xS$  systems,<sup>11</sup> will provide the means by which such an investigation can be accomplished.

#### IV. CONCLUSIONS

Our results indicate the Mn (Co)  $L_{3,2}$ -edge white-line spectra increase linearly in intensity with magnetic-transition-metal concentration for  $Zn_{1-x}Mn_xY$  ( $Y=S,Se$ ) and

for  $Zn_{1-x}Co_xS$ , in proportion to the strength of the Mn (Co)  $3d(t_2)$ -S  $3p$  hybridized antibonding states for the sulfides, and of the Mn  $3d(t_2)$ -Se  $4p$  hybridized states for the selenides. We find, based on the analysis of the rate of increase of the magnetic-transition-metal  $L_{3,2}$ -edge white-line intensities, that magnetic-transition-metal  $3d(t_2)$ -anion  $p$  hybridization is greatest for  $Zn_{1-x}Co_xS$ , intermediate for  $Zn_{1-x}Mn_xS$  and least for  $Zn_{1-x}Mn_xSe$ . We infer that this is due to the differences in energy between the Mn (Co)  $3d(t_2)$  and anion  $p$  states in these alloys. Our results from analysis of Mn and Co  $K$ -edge EXAFS spectra show significant local structure relaxation based on results showing that the NN  $M$ -S bond lengths remained essentially independent of  $x$  in  $Zn_{1-x}Mn_xS$  and  $Zn_{1-x}Co_xS$  alloys, respectively. We infer this to be due to strong hybridization of  $Mn^{2+}$  and  $Co^{2+}$   $3d$  orbitals having  $t_2$  symmetry with anion  $3p$  or  $4p$  orbitals, thereby leaving fewer anion  $p$  orbitals available for tetrahedral bonding, and weakening the  $sp^3$  bonds in these materials.

#### ACKNOWLEDGMENTS

We would like to thank Professor J. K. Furdyna and U. Debska for providing the samples used in this study. One of the authors (W.F.P.) acknowledges support from the National Science Council of the Republic of China under Contract No. NSC85-2112-M-032-003. This work was performed on the HSGM beamline at SRRC. We also thank the staff of SRRC for their technical support.

- 
- <sup>1</sup>Diluted Magnetic Semiconductors, Semiconductors and Semimetals Vol. 25, edited by J. K. Furdyna and J. Kossut (Academic, New York, 1988).
- <sup>2</sup>Diluted Magnetic Semiconductors, edited by M. Jain (World Scientific, Singapore, 1991).
- <sup>3</sup>M. Taniguchi, M. Fujisawa, T. Mori, I. Souma, and Y. Oka, Solid State Commun. **62**, 431 (1987).
- <sup>4</sup>R. Weidemann, H. E. Gumlich, M. Kupsch, H. U. Middelmann, and U. Becker, Phys. Rev. B **45**, 1172 (1992).
- <sup>5</sup>B. E. Larson, K. C. Hass, H. Ehrenreich, and A. E. Carlsson, Phys. Rev. B **37**, 4137 (1988).
- <sup>6</sup>S. H. Wei and A. Zunger, Phys. Rev. B **37**, 8958 (1988).
- <sup>7</sup>R. A. Mayanovic, R. J. Sladek, and U. Debska, Phys. Rev. B **38**, 1311 (1988).
- <sup>8</sup>W. F. Pong, R. A. Mayanovic, B. A. Bunker, J. K. Furdyna, and U. Debska, Phys. Rev. B **41**, 8440 (1990).
- <sup>9</sup>R. A. Mayanovic, W. F. Pong, and B. A. Bunker, Phys. Rev. B **42**, 11 174 (1990).
- <sup>10</sup>W. F. Pong, R. A. Mayanovic, K. T. Wu, P. K. Tseng, B. A. Bunker, A. Hiraya, and M. Watanabe, Phys. Rev. B **50**, 7371 (1994).
- <sup>11</sup>W. F. Pong *et al.* (unpublished).
- <sup>12</sup>F. M. F. de Groot, J. C. Fuggle, B. T. Thole, and G. A. Sawatzky, Phys. Rev. B **42**, 5459 (1990).
- <sup>13</sup>G. van der Laan and I. W. Kirkman, J. Phys. Condens. Matter **4**, 4189 (1992).
- <sup>14</sup>K. Lawniczak-Jablonska, R. J. Iwanowski, Z. Golacki, A. Traverse, S. Pizzini, A. Fontaine, I. Winter, and J. Hormes, Phys. Rev. B **53**, 1119 (1996).
- <sup>15</sup>G. van der Laan, J. Zaanen, G. A. Sawatzky, R. Karnatak, and J. M. Esteve, Phys. Rev. B **33**, 4253 (1986); G. van der Laan, B. T. Thole, G. A. Sawatzky, and M. Verdager, *ibid.* **37**, 6587 (1988).
- <sup>16</sup>A. Lewicki, A. I. Schindler, J. K. Furdyna, and W. Giriat, Phys. Rev. B **40**, 2379 (1989); T. M. Giebultowicz, P. Klosowski, J. J. Rhyne, T. J. Udovic, J. K. Furdyna, and W. Giriat, *ibid.* **41**, 504 (1990); A. Lewicki, A. I. Schindler, I. Miotkowski, J. K. Furdyna, and W. Giriat, *ibid.* **41**, 4653 (1990); P. M. Shand, A. Lewicki, I. Miotkowski, B. C. Crooker, and J. K. Furdyna, *ibid.* **44**, 6152 (1991).
- <sup>17</sup>T. M. Giebultowicz, J. J. Rhyne, and J. K. Furdyna, J. Appl. Phys. **61**, 3537 (1987); D. U. Bartholomew, E. K. Suh, S. Rodriguez, A. K. Ramdas, and R. L. Aggarwal, Solid State Commun. **62**, 235 (1987); V. Spasojevic, A. Bajorek, A. Szytula, and W. Giriat, J. Magn. Magn. Mater. **80**, 183 (1989).
- <sup>18</sup>P. C. Kemeny and N. J. Shevchik, Solid State Commun. **17**, 255 (1975).
- <sup>19</sup>See Appendix B, *Unoccupied Electronic States*, edited by J. C. Fuggle and J. E. Inglesfield (Springer-Verlag, Berlin, 1992).
- <sup>20</sup>N. J. Shevchik, Phys. Rev. Lett. **33**, 1336 (1974).
- <sup>21</sup>Note that the energy range of integrated intensities of the Co  $L_3$  edge for  $Zn_{1-x}Co_xS$  (777.6–781.8 eV) is larger than that of the Mn  $L_3$  edge for  $Zn_{1-x}Mn_xY$  (638.3–641.7 eV).
- <sup>22</sup>M. Zinnal-Starnawska, J. Lazewski, A. Kisiel, F. Boscherini, S. Pascarelli, and W. Giriat, Acta Phys. Pol. A **86**, 763 (1994).
- <sup>23</sup>K. Lawniczak-Jablonska and Z. Golacki, Acta Phys. Pol. A **86**, 727 (1994).

- <sup>24</sup>D. R. Yoder-Short, U. Debska, and J. K. Furdyna, *J. Appl. Phys.* **58**, 4056 (1985).
- <sup>25</sup>P. Maheswaranathan, R. J. Sladek, and U. Debska, *Phys. Rev. B* **31**, 5212 (1985).
- <sup>26</sup>S. B. Qadri, E. F. Skelton, A. W. Webb, E. R. Carpenter, Jr., M. W. Schaefer, and J. K. Furdyna, *Phys. Rev. B* **35**, 6868 (1987).
- <sup>27</sup>J. Spalek, A. Lewicki, Z. Tarnawski, J. K. Furdyna, R. R. Galazka, and Z. Obuszko, *Phys. Rev. B* **33**, 3407 (1986).